

RFWNet: A Lightweight Remote Sensing Object Detector Integrating Multi-Scale Receptive Fields and Foreground Focus Mechanism

Yujie Lei¹, Wenjie Sun¹, Sen Jia², Qingquan Li³ and Jie Zhang^{1,4} *

¹ College of Information and Electrical Engineering, China Agricultural University, Beijing 100083, China.

² College of Computer Science and Software Engineering, Shenzhen University, Shenzhen 518060, China.

³ Shenzhen Key Laboratory of Spatial Smart Sensing and Services, Shenzhen University, Shenzhen 518060, China.

⁴ Key Laboratory of Agricultural Machinery Monitoring and Big Data Applications, Ministry of Agriculture and Rural Affairs, Beijing 100083, China.
jiezhang@cau.edu.cn

Abstract. Challenges in remote sensing object detection (RSOD), such as high inter-class similarity, imbalanced foreground-background distribution, and the small size of objects in remote sensing images significantly hinder detection accuracy. Moreover, the trade-off between model accuracy and computational complexity poses additional constraints on the application of RSOD algorithms. To address these issues, this study proposes an efficient and lightweight RSOD algorithm integrating multi-scale receptive fields and foreground focus mechanism, named RFWNet. Specifically, we proposed a lightweight backbone network Receptive Field Adaptive Selection Network (RFASNet), leveraging the rich context information of remote sensing images to enhance class separability. Additionally, we developed a Foreground Background Separation Module (FBSM) consisting of a background redundant information filtering module and a foreground information enhancement module to emphasize critical regions within images while filtering redundant background information. Finally, we designed a loss function, the Weighted CIoU-Wasserstein (WCW) loss, which weights the IoU-based loss by using the Normalized Wasserstein Distance to mitigate model sensitivity to small object position deviations. Experimental evaluations on the DOTA V1.0 and NWPU VHR-10 datasets demonstrate that RFWNet achieves advanced performance with 6.0M parameters and can achieve 52 FPS.

Keywords: Object detection, Lightweight, Foreground background separation, Receptive field adaptive selection, Remote sensing.

1 Introduction

Rapid development of deep learning has significantly enhanced computer vision technology, particularly in the field of object detection, which has wide application potential

in automatic driving, environmental monitoring, and smart agriculture [1]. With the progress in airborne and satellite sensors, high spatial resolution (HSR) remote sensing images have become increasingly accessible. Therefore, RSOD based on deep learning has gained prominence, playing a critical role in various domains, including ecological monitoring, smart agriculture, and disaster forecasting [2].

However, remote sensing objects are complex and variable in scale, features, and distribution, which makes remote sensing object detection face challenges such as high inter-class similarity, small target size, and imbalance between foreground and background distribution [3], [4]. High inter-class similarity can lead to misclassification without referring to sufficient contextual information. Additionally, the proportion of background and the small size of targets further complicate accurate detection [5].

To address these challenges, many high-precision RSOD algorithms have been proposed, significantly enhancing the accuracy of RSOD [6], [7], [8]. For instance, Li et al. introduced LSKNet [9], which dynamically adjusts the receptive field size during the feature extraction process to effectively manage variations in background information requirements that vary from object to object. However, LSKNet does not sufficiently address the issue of unbalanced foreground-background distribution. Lv et al. proposed a detection model tailored for small objects, which effectively mitigates the small-target detection challenge [10], yet it also suffers from the problem that the model tends to predict targets as background. Rao et al. proposed a cross-grid label assignment to enhance positive samples to alleviate the unbalanced foreground-background distribution issue, but the limited exploration of target contextual information restricts its accuracy in detecting small and high interclass similarity targets [11]. Additionally, most of the existing research on RSOD primarily focuses on improving accuracy while neglecting computational complexity, leading to methods with high accuracy but excessive model parameters and slow inference speed [12]. For example, RVSA [6] achieved 70.67% accuracy on the DIOR-R dataset, but its parameter is as large as 113.13M, making it unsuitable for deployment on mobile devices. With the development of UAVs across various fields, the demand for real-time RSOD algorithms has intensified, and the balance between model accuracy and speed has become increasingly critical [13]. Consequently, developing lightweight models that can effectively address the challenges of high inter-class similarity, imbalanced foreground-background distribution, and the small size of objects in RSOD has become the key focus in this area.

To address the challenges of high inter-class similarity, small target size, and unbalanced foreground-background distribution in RSOD, while keeping a balance between accuracy and model complexity, we propose a lightweight and high-precision RSOD model, RFWNet. The principal contributions of this study are outlined as follows:

- 1) We propose a lightweight and efficient oriented object detector for object detection of remote sensing images. By optimizing the feature space of targets at different scales while ensuring lightweight, RFWNet achieves advanced detection accuracy with 6.0M parameters and achieves 52 FPS.

- 2) We design a lightweight backbone Receptive Field Adaptive Selection Network (RFASNet) as the model backbone based on convolutions with different expansion rates. This lightweight backbone is designed to fully utilize the context information of

targets based on adaptive selection of receptive fields, thereby increasing the interclass discrete distance.

3) We develop a Foreground Background Separation Module (FBSM), which consists of a background redundant information filtering module and a foreground information enhancement module to extract more effective features while filtering out redundant information.

4) We propose a novel boundary box regression loss function, Weighted CIoU-Wasserstein (WCW) loss, which weights the IoU-based loss by using the Normalized Wasserstein Distance to mitigate the models's sensitivity to small target positional deviations.

2 Related Work

2.1 Large Receptive Field Network

The large receptive field is critically necessary for HSR remote sensing images with large spatial dimensions. In the field of computer vision, large receptive fields have been identified as key factors contributing to the success of Vision Transformer and Swin Transformer models [14], [15], [16]. This feature significantly improves the model's ability to capture global contextual information. Similarly, large kernel convolution (LKC), a strategy designed to expand the receptive field in CNN-based models, has demonstrated competitive performance on par with Transformer-based models. By increasing the convolution kernel size, LKC enables object detection models to capture features over a broader area, thus improving their ability to interpret and characterize complex images.

However, expanding the convolution kernel size typically results in a substantial increase in computational complexity and parameters [17]. To address this challenge, techniques such as grouped convolution have been employed to mitigate the computational cost of LKC while preserving its large receptive field. The success of CNN-based models like ConvNeXt also validates the strong potential and competitiveness of LKC in object detection [18], [19].

The advantage of LKC in capturing richer spatial contextual information is particularly significant when dealing with complex scenes, such as high-resolution remote sensing images [20]. However, its application in lightweight RSOD methods remains limited. While LSKNet is the first to introduce LKC in RSOD, its model size restricts its deployment potential on mobile and embedded platforms. In addition, for targets with distinct local features, smaller receptive fields tend to be more effective, and large receptive fields are unnecessary. Therefore, this study devotes to develop a lightweight RSOD method that incorporates adaptive receptive fields, thereby enhancing the model's ability to understand and detect complex remote sensing image content while maintaining a lightweight architecture.

2.2 Lightweight Remote Sensing Object Detection Models

The growing demand for efficient real-time detection in environments characterized by limited resources like unmanned aerial vehicles (UAVs), has spurred significant

interest in lightweight RSOD research. By streamlining the network structures, optimizing the parameter configuration, and introducing efficient computational units, lightweight RSOD models have effectively reduced computational complexity and model parameters while maintaining detection accuracy. As a result, significant advancements have been achieved in the area of lightweight RSOD.

A series of compact and efficient network architectures are applied to the construction of RSOD models, such as MobileNet and ShuffleNet [21], [22]. These networks employ lightweight techniques like depth-separable convolution and point-by-point group convolution, effectively reducing model parameters and computational costs while preserving strong feature extraction capabilities.

On the other hand, researchers have developed various lightweight RSOD models by improving the general lightweight object detection framework based on remote sensing image characteristics. Lin et al. proposed an efficient remote sensing object detector based on YOLOv5 and decoupled attention head, which achieves a better equilibrium between the detection performance and the speed [23]. Dong et al. proposed an efficient lightweight remote sensing object detector ELNet, which improves the model's accuracy while reducing the parameters [24]. Zhu et al. introduced a selective feature enhancement block (SFEB) and a context transformer block (CTB) based on YOLOv5n, which improves the model's ability for small objects detection [25]. Additionally, researchers have explored model compression techniques, such as knowledge distillation [26] and pruning [27], which further compress model size and accelerate inference speed without compromising accuracy.

Lightweight object detection models often face the challenge of decreasing accuracy, a tradeoff that becomes particularly pronounced when applied to the complex nature of remote sensing images [28]. While the above studies have achieved a good balance between lightweight and model accuracy, they have only considered fewer remote sensing characteristics and there is still some room for improvement.

3 Methodology

3.1 Overall framework

Same as other object detection networks, RFWNet consists of three parts: backbone, neck and head. The backbone consists of RFASNet, Spatial Pyramid Pooling-Fast (SPPF) and FBSM. Neck consists of Feature Pyramid Network (FPN) [29] and Path Aggregation Network (PANet) [30]. Head consists of three scales of detection heads that return the category and coordinates of targets. The parameter count of RFWNet is 6.0M, the network architecture is shown in Fig. 1.

3.2 Receptive Field Adaptive Selection Network

Different sizes of receptive fields are accompanied by varying target context information [31]. The rich contextual information provided by large receptive fields offers a significant advantage in recognizing confusable classes and large area features. However, large receptive fields are not always necessary. For targets with distinct local features, a smaller receptive field is often more effective. To address the challenge of inter-

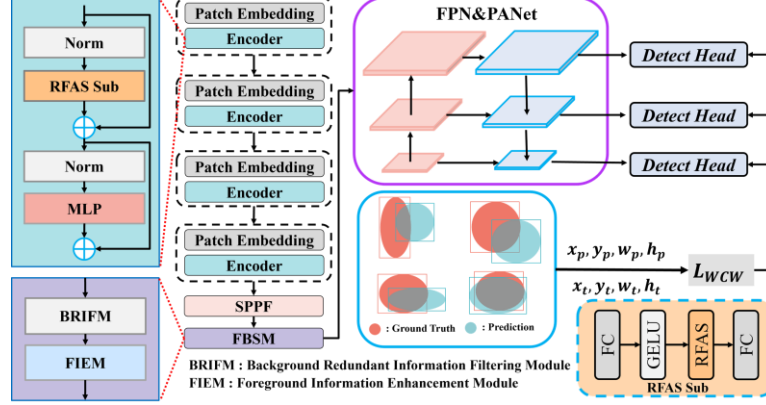


Fig. 1. RFWNet structure diagram. RFWNet consists of the backbone (RFASNet), the feature pyramid network and three detection heads. L_{WCW} acts on the regression branch of detection heads.

class similarity and more effectively capture target-specific contextual information, we propose the Receptive Field Adaptive Selection network (RFASNet) as backbone. This network is designed to adaptively select the appropriate receptive field size based on the characteristics of the target. As shown in Fig.1, the RFASNet consists of normalization, Receptive Field Adaptive Selection Module (RFASM), and MLP, the core of RFASM is RFAS Block. The network structure of RFAS Block as shown in Fig. 2.

Specifically, RFAS Block consists of three parts: multiple different receptive field branches, feature selection and feature aggregation. Multiple different receptive field branches are composed of multi-scale convolutions, and these convolutional layers can extract features with different receptive fields from the input image to provide rich context information. Since large receptive fields are often realized by large kernel convolution, but large kernel convolution often brings large computation, we decompose the large kernel convolution into standard convolution and dilated convolution to reduce the model computation while guaranteeing large receptive fields.

We superimpose the features of two smaller receptive fields and the features of two larger receptive fields respectively, and concatenate the resulting features F_{srf} and F_{lrf} in the channel dimension to obtain a mixed feature of multiple receptive fields F_{mrf} .

$$F_{srf} = W_{3,3} \left(W_{3,1}(x) \right) + W_{3,1}(x) \quad (1)$$

$$F_{lrf} = W_{3,5} \left(W_{5,1}(x) \right) + W_{5,1}(x) \quad (2)$$

$$F_{mrf} = [F_{srf}, F_{lrf}] \quad (3)$$

where $W_{a,b}$ denotes the convolution operation, a denotes the convolution kernel size, b denotes the dilation rate, X denotes the input image or feature map, and the square bracket denotes the concatenate operation.

To select the most suitable receptive field for the target, we perform pooling operations on multi receptive field mixed features F_{mrf} to highlight key information, providing information sources for subsequent feature selection and feature aggregation. The feature selection module receives the output feature map F_{mp} and F_{ap} from the pooling operation, processes it through the convolution layer, and then generates the weight matrix through the Sigmoid activation function w .

$$w = \sigma \left(W_{7,1}([F_{mp}, F_{ap}]) \right) \quad (4)$$

Based on the weight matrix w , the feature aggregation module aggregates F_{srf} and F_{trf} from different receptive field branches by weighted summation operation to obtain the final attention feature map. Finally, the attention feature map is multiplied by the input X to enhance or suppress the input feature map.

$$F_{out} = x * W_{1,1}(w_1 * F_{srf} + w_2 * F_{trf}) \quad (5)$$

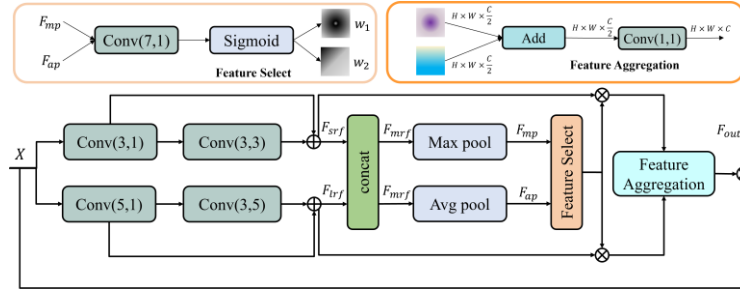


Fig. 2. RFASNet Block structure diagram. Corresponding to RFAS in RFASM in Fig. 1.

3.3 Foreground Background Separation Module

In remote sensing images, complex background often occupies a large proportion, while the proportion of the foreground is small [32]. To filter redundant background information and enhance the focus on key information, we design a Foreground Background Separation Module (FBSM), as shown in Fig. 3. FBSM includes two parts: Background Redundant Information Filtering Module (BRIFM) and Foreground Information Enhancement Module (FIEM). Firstly, BRIFM divides the image into multiple regions, and then filters out the irrelevant regions according to the key-value pairs to filter the redundant information. Secondly, FIEM dynamically adjusts the importance of each pixel on the result of BRIFM, and enhances the model's attention to key areas.

Specifically, BRIFM mainly consists of linear transformation and region filtering. For a given input feature map $X \in \mathbb{R}^{H \times W \times C}$, it is first divided into multiple non-overlapping regions containing $\frac{H \times W}{s^2}$ feature vectors, then X can be reshape as $X_r \in \mathbb{R}^{s^2 \times \frac{H \times W}{s^2} \times C}$. Next, the query tensor Q , the key tensor K , and the value tensor V , are obtained by linear transformation mapping, and the mean value of each tensor in each region is computed to capture the overall features of each region. Subsequently, use TopkRouting to select the most relevant K key-value pairs, return the routing weight

r_w and index r_l , and assemble the key-value pairs K_{sel} and V_{sel} based on the indexes and weights. Then input the dot product of Q and K_{sel} into the Softmax function to get the attention weight matrix w_{BRIFM} . Finally, the filtering of irrelevant region is realized by multiplying V_{sel} with w_{BRIFM} .

The FIEM is based on the results of the BRIFM, which mainly consists of pooling, convolutional and Sigmoid layers. Specifically, the features F processed by BRIFM are used as inputs for max pooling and average pooling, using the channel-based pooling layer to efficiently extract spatial relations. Then the outputs of pooling layers F_m and F_a are converted into a single-channel spatial attention map by a convolutional layer. Finally, the output of the convolutional layer is converted to an attention weight w_{FIEM} using a sigmoid function, which is applied to the input feature map F to enhance the features of important regions.

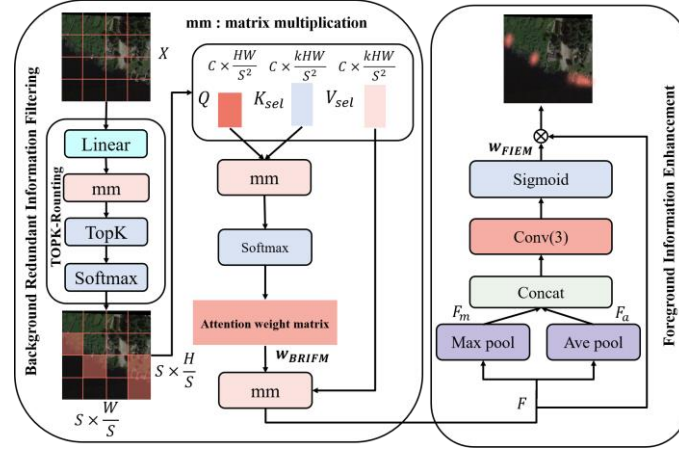


Fig. 3. FBSM structure diagram. FBSM consists of the Background Redundant Information Filtering Module (BRIFM) and the Foreground Information Enhancement Module (FIEM).

3.4 Weighted CIoU-Wasserstein loss

Accurately detecting large number of small remote sensing targets is one of the main challenges of RSOD [33]. Limited by the calculation formula of the IoU itself, traditional IoU-based measurement methods are susceptible to the positional deviation of small objects [34]. As shown in Fig. 4, the IoU drops significantly when the small target has only a small positional deviation, this is unfriendly to RSOD. To address the problem, we propose a Weighted CIoU-Wasserstein loss (WCWloss).

Normalized Wasserstein Distance loss (NWD loss) is based on Wasserstein distance for metrics and is specifically designed to solve the problem of small target detection [35]. Firstly, the predicted boxes and labels are transformed into 2D Gaussian distributions to describe the weight distribution of different pixels in the bounding box. Secondly, NWD Loss measures the similarity or difference between the predicted bounding box and the real bounding box by considering their difference in probability distribution. NWD loss not only relies on the spatial correlation between pixels, but also takes into account the location and size information of the bounding box, which is scale-

insensitive and friendly for small target detection. Therefore, we further optimize the model's sensitivity to small target positional deviation by weighted combining NWD Loss based on CIoU, which is calculated as shown in Eq. (6).

$$L_{WCW} = \gamma * L_{CIoU} + \beta * L_{nwd} \quad (6)$$

where L_{CIoU} is the CIoU loss, the calculation process is shown in Equation (7). L_{nwd} is the NWD loss, the calculation process is shown in Equation (8-9). γ and β are the weights of L_{CIoU} and L_{nwd} , and both of them are 0.5 by default.

$$L_{CIoU} = 1 - IoU + \frac{d^2}{c^2} + \frac{v^2}{(1-IoU)+v} \quad (7)$$

$$W_2^2(N_a, N_b) = \left\| \left(\left[c_{xa}, c_{ya}, \frac{W_a}{2}, \frac{H_a}{2} \right]^T, \left[c_{xb}, c_{yb}, \frac{W_b}{2}, \frac{H_b}{2} \right]^T \right) \right\|_2^2 \quad (8)$$

$$L_{nwd} = 1 - \exp\left(-\frac{\sqrt{W_2^2(N_a, N_b)}}{c}\right) \quad (9)$$

where d represents the distance between the centroid of the prediction box and the centroid of the label, v is the correction factor, c represents the diagonal distance of the smallest outer rectangle of the two rectangular boxes, $(c_{xa}, c_{ya}, W_a, H_a)$ and $(c_{xb}, c_{yb}, W_b, H_b)$ are predicted bounding boxes and real labels.

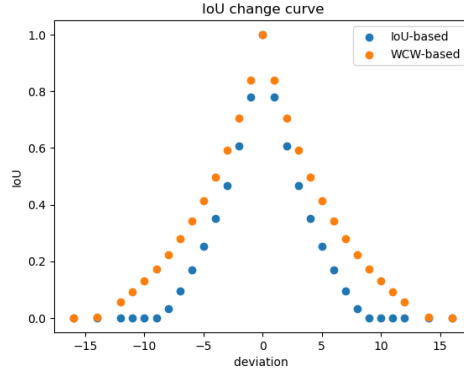


Fig. 4. IoU variation of 16×16 target position deviation under different similarity measures.

4 Experiments

4.1 Datasets

The DOTA V1.0 dataset is a large-scale RSOD dataset proposed by Wuhan University [36], which includes 2806 images, 15 categories. These 15 categories are small vehicle (SV), large vehicle (LV), plane (PL), storage tank (ST), ship (SH), harbor (HA), ground track field (GTF), soccer ball field (SBF), tennis course (TC), swimming pool (SP),

baseball diamond (BD), roundabout (RA), basketball court (BC), bridge (BR), helicopter (HE). To facilitate train and test, we cropped these images to images with a resolution of 1024×1024 .

The NWPU VHR-10 dataset is a RSOD dataset with a total of 800 HSR satellite images [37]. These images are rigorously manually labeled by experts to ensure the accuracy of the labeled information. It includes 10 classes, namely airplane (AE), ship (SP), tennis court (TC), storage tank (ST), the harbor (HR), baseball diamond (BD), basketball court (BC), ground track field (GT), vehicle (VE) and bridge (BE).

4.2 Experiments Setup

Implementation Detail. All experiments in this study were conducted on the Ubuntu system based on the Pytorch framework, with Pytorch version 1.11.0, Ubuntu version 20.04, Python version 3.8, and Cuda version 11.3. The graphics card is RTX3090, and the CPU is Intel (R) Xeon (R) Platinum 8255C @ 2.50GHz. The initial learning rate is 0.001, with 16 batch sizes and 100 epochs. For the DOTA dataset, we cut the original image to a fixed size of 1024×1024 , and the overlap between adjacent images is 200. None of the experiments in this paper use pre-training weights. The hyperparameters are set as: $\gamma = 0.5$, $\beta = 0.5$.

Evaluation Metrics. Average Precision (AP), Precision, Recall and mean Average Precision (mAP) are widely used evaluation indicators for RSOD, and they are also selected as experimental evaluation indicators in this study.

4.3 Comparison Experiments

To evaluate the performance of the RFWNet model more comprehensively and accurately, a comparison experiment of the model was designed in this study. RFWNet compared with the mainstream RSOD models on DOTA V1.0 and NWPU VHR-10 datasets.

Table 1. Comparison experiment results of NWTU-VHR 10.

Methods	AE	SP	ST	BD	TC	BC	GT	HR	BE	VE	mAP
F-RCNN [38]	82.8	77.5	52.5	96.3	62.9	68.8	98.4	82.5	78.8	63.8	76.4
M-RCNN [39]	93.2	75.5	92.9	90.4	90.3	91.2	95.2	75.2	60.6	74.2	83.9
EGAT-LSTM [40]	97.3	96.7	97.2	96.5	86.6	94.5	94.2	86.2	80.1	90.8	92.0
YOLOX [41]	99.4	84.3	92.9	99.9	94.8	95.8	100	94.8	72.2	88.9	92.3
MEDNet [42]	99.2	94.4	82.2	98.5	95.4	95.2	98.3	88.1	75.1	89.3	91.6
YOLO-PDNet [43]	99.0	88.2	97.7	97.2	94.2	93.4	99.5	90.0	83.3	93.5	93.6
SOD-YOLOv10 [44]	99.5	99.2	90.1	96.7	91.4	90.6	96.5	95.8	92.0	72.8	93.2
RS-YOLO [45]	99.9	94.1	96.6	97.8	93.8	92.7	97.6	89.5	84.7	92.3	93.9
ours	99.8	95.3	83.0	97.9	98.9	98.7	99.4	95.7	90.3	94.2	95.3

Experimental results on the NWPU-VHR 10 Dataset. To verify the effectiveness of our proposed method, comparative experiments are conducted on the HSR RSOD dataset. The quantitative results from Table 1 show that RFWNet achieves advanced results with a mAP of 95.3% on this benchmark dataset. In terms of individual category performance, RFWNet achieves optimal or sub-optimal accuracy on 4 categories of NWPU-VHR 10. Fig. 5 shows the detection results of RFWNet and the baseline on the NWPU-VHR 10 dataset. Based on this, we qualitatively discuss the detection ability of

RFWNet. It can be seen that when dealing with complex remote sensing images, our proposed RFWNet can effectively avoid misdetection and missed detection.

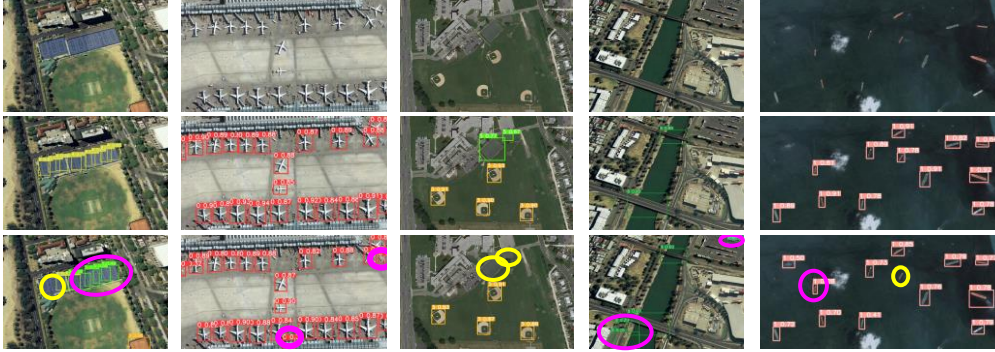


Fig. 5. Comparison of detection results of NWPU VHR-10. The top row is original images, the middle row is RFWNet, and the bottom row is Baseline. The yellow circle represents missed detection, the purple circle represents wrong detection.

Experimental results on the DOTA V1.0 Dataset. To verify the robustness of our proposed method, comparative experiments are conducted on the HSR RSOD dataset DOTA V1.0. The quantitative results from Table 2 show that RFWNet achieves advanced results with a mAP of 73.2% on this benchmark dataset. In terms of individual category performance, RFWNet achieves optimal or sub-optimal accuracy on 8 out of 15 categories of DOTA V1.0. Fig. 6 shows the detection results of RFWNet and the baseline on the DOTA V1.0 dataset. It can be seen that RFWNet has better detection ability for remote sensing targets of different scales in different dense scenes.

Table 2. Comparison experiment results of DOTA V1.0.

Class	SV	LV	PL	ST	SH	HA	GTF	SBF	TC	SP	BD	RA	BC	BR	HE	mAP
FMSSD [46]	69.2	73.6	89.1	73.3	76.9	72.4	67.9	52.7	90.7	80.6	81.5	67.5	82.7	48.2	68.9	72.4
RetinaNet	73.8	63.5	88.3	65.9	77.7	68.9	59.1	48.7	90.4	71.6	77.8	61.8	78.6	47.9	38.2	67.5
ICN [47]	73.5	65.0	90.0	84.8	78.2	73.5	73.3	57.2	90.8	70.2	77.7	62.1	79.1	53.3	58.1	72.5
CMR [48]	79.2	65.9	88.9	81.9	78.1	73.0	64.0	46.5	90.1	70.0	81.5	62.9	77.5	52.9	58.3	71.4
IoU-Ada [49]	76.3	72.6	88.6	76.2	84.1	74.1	67.0	57.1	90.7	66.4	80.2	66.7	81.0	53.2	56.9	72.7
F-RCNN	78.0	65.6	89.0	81.7	78.0	72.6	60.8	47.1	90.1	70.9	75.8	61.5	77.3	53.5	59.5	70.8
ours	69.2	87.7	92.3	72.6	90.0	83.3	74.1	58.1	94.3	64.1	81.5	60.2	65.0	49.6	56.2	73.2

Inference speed. To better evaluate the lightweight of RFWNet, we conducted inference speed test experiments on the testset of DOTA V1.0 dataset. Consistent with the training, the image of the test set is also cropped to equal-size images of 1024×1024 . The results show that the RFWNet inference of a single image takes only 19.1 ms, achieving a FPS of 52. Table 3 demonstrates the comparison results with other models, and it can be seen that RFWNet has an excellent performance in both parameters and inference speed.

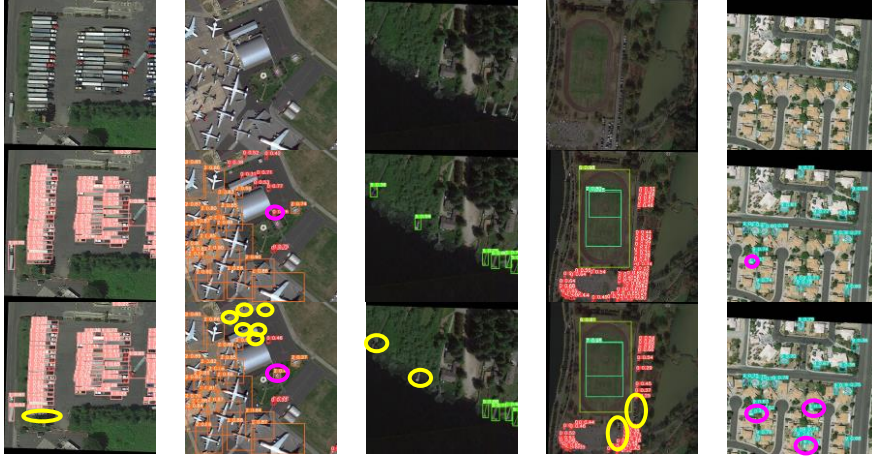


Fig. 6. Detection results comparison on DOTA v1.0. The top row is original images, the middle row is RFWNet, and the bottom row is Baseline. The yellow circle represents missed detection, the purple circle represents wrong detection.

Table 3. Parameter and Inference Speed Comparison Experiments.

Methods	EfficientDet [50]	EL-YOLO	FSoDNet [51]	RetinaNet	RFBNet	ours
FPS \uparrow	23.8	24.0	18.2	11.1	33.3	52.4
Parameter/M \downarrow	83.9	4.3	232.2	147.2	185.1	6.0

4.4 Ablation Study

The influence of WCW’s hyperparameters. In this section, we discuss the effectiveness of the WCW loss and the effect of the two hyperparameters γ and β on the accuracy based on the NWPU VHR-10 dataset. The experimental results with different weighting ratios are shown in Table 4. When both γ and β are 0.5, it can achieve the optimal performance of 95.3%, which is 1.6% higher than using L_{Clou} . We believe that this ratio can effectively reduce the sensitivity to small target position deviation while ensuring the effectiveness of bounding box regression for medium and large targets. Therefore, we used 0.5 as the default value of γ and β in all the experiments.

Table 4. Ablation experiment results of hyperparameters.

γ	β	mAP
1.0	0.0	93.7%
0.9	0.1	94.6%
0.8	0.2	93.9%
0.7	0.3	94.1%
0.6	0.4	93.3%
0.5	0.5	95.3%
0.0	1.0	94.2%

Effectiveness of RFASNet. In this section, we discuss the effectiveness of RFASNet. Table 5 shows that compared to the baseline network, our improved backbone network

RFASNet brings 3.2% and 3.9% accuracy improvement on the two benchmark datasets, respectively. Moreover, when combined with other improvements, RFASNet can also bring some performance gains. The experimental results illustrate that RFASNet is able to accurately consider the target features and effectively solve the misclassification problem caused by high inter-class similarity. Therefore, we use RFASNet as the model backbone network in the subsequent experiments.

Effectiveness of FBSM. In this section, we discuss the effectiveness of FBSM. Table 5 shows that compared to RNet, our proposed FBSM brings 0.8% and 0.9% improvement in mAP on the two datasets, respectively. In addition, when combined with RWNNet, FBSM can also bring some performance improvement. The above experimental results illustrate that FBSM can filter the redundant background information and improve the focus on the foreground during the training process, effectively solving the foreground-background imbalance problem.

Attention Visualization. Fig.7 demonstrates the feature extraction ability of models before and after the improvement through heatmap visualization. The baseline focuses too much on certain irrelevant regions, such as background noise or image edges. In contrast, RFWNet better suppresses the interference of background regions, reduces the focus on irrelevant regions, and extracts more accurate and enriched features, which improves detection accuracy.

Table 5. Ablation experiment results of improvements.

Model	RFASNet	FBSM	WCW loss	mAP/DOTA	mAP/NWPU
Baseline	×	×	×	69.0%	88.9%
RNet	√	×	×	72.2% (+3.2%)	92.8% (+3.9%)
RFNet	√	√	×	73.0% (+3.9%)	93.7% (+4.8%)
RWNNet	√	×	√	72.5% (+3.5%)	94.2% (+5.3%)
RFWNet	√	√	√	73.2% (+4.2%)	95.3% (+6.4%)

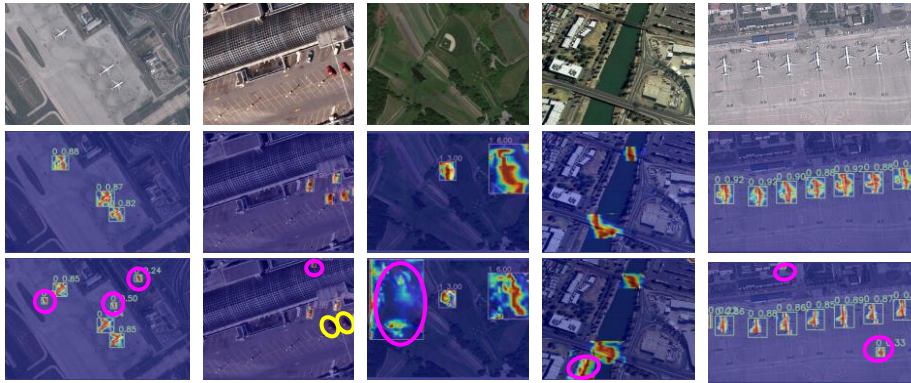


Fig. 7. Attention visualization chart. The top row is original images, the middle row is RFWNet, and the bottom row is Baseline. The yellow circle represents missed detection, the purple circle represents wrong detection.

5 Conclusion

In this study, we propose RFWNet, an efficient and lightweight remote sensing object detection algorithm designed to address the challenges of high inter-class similarity, foreground-background imbalance, and small size of objects in the high spatial resolution remote sensing object detection. RFWNet introduces optimizations in both feature extraction and bounding box regression. Specifically, we developed a receptive field adaptive selection network as the model backbone to capture the context information of remote sensing targets effectively. Secondly, we designed a foreground-background separation model FBSM to enhance the focus on foreground information while filtering background redundant information. Finally, we designed Weighted CIoU-Wasserstein loss as the regression loss function to reduce the model's sensitivity to small target position deviation. The effectiveness of these innovations was validated on two representative datasets. The comprehensive experimental results demonstrate that RFWNet achieves advanced detection results while maintaining an optimal balance between accuracy and computational efficiency.

Acknowledgments. This work was supported by Major Science and Technology Special Program of Yunnan Province (202202AE090034), the National Key Research and Development Program (2022YFF0713002, 2021YFD1901001), Project (GEMLab-2023001) supported by MNR Key Laboratory for Geo-Environmental Monitoring of Greater Bay Area, Project of Agriculture and Rural Affairs Bureau of Chun'an County, Hangzhou Chiti, Zhejiang Province, China. (ZJYGZF [2022]009).

Disclosure of Interests. The authors have no competing interests to declare that are relevant to the content of this article.

References

1. Bustos N., Mashhadi M., Lai-Yuen S.K., Sarkar S., Das T.K.: A systematic literature review on object detection using near infrared and thermal images. *Neurocomputing*. 560. 126804 (2023).
2. Luo L., Wang X., Guo H., Lasaponara R., Zong X., Masini N., Wang G., Shi P., Khatteli H., Chen F., Tariq S., Shao J., Bachagha N., Yang R., Yao Y.: Airborne and spaceborne remote sensing for archaeological and cultural heritage applications: A review of the century (1907–2017). *Remote Sensing of Environment*. 232. 111280 (2019).
3. Wang S., Huang S., Liu S., Bi Y.: Not just select samples, but exploration: Genetic programming aided remote sensing target detection under deep learning. *Applied Soft Computing*. 145. 110570 (2023).
4. Wang Y., Zhang W., Zhang Z., Gao X., Sun X.: Multiscale Multiinteraction Network for Remote Sensing Image Captioning. *IEEE Journal of Selected Topics in Applied Earth Observations and Remote Sensing*. 15. 2154 (2022).
5. Zhao W., Zhao Z., Xu M., Ding Y., Gong J.: Differential multimodal fusion algorithm for remote sensing object detection through multi-branch feature extraction. *Expert Systems with Applications*. 265. 125826 (2025).

6. Wang D., Zhang Q., Xu Y., Zhang J., Du B., Tao D., Zhang L.: Advancing Plain Vision Transformer Toward Remote Sensing Foundation Model. *IEEE Transactions on Geoscience and Remote Sensing*. 61. 1 (2023).
7. Yang X., Zhou Y., Zhang G., Yang J., Wang W., Yan J., Zhang X., Tian Q.: THE KFIOU LOSS FOR ROTATED OBJECT DETECTION. In: *International Conference on Learning Representations* (2023).
8. Yang X., Yang X., Yang J., Ming Q., Wang W., Tian Q., Yan J.: Learning High-Precision Bounding Box for Rotated Object Detection via Kullback-Leibler Divergence. In: *Proceedings of the 35th International Conference on Neural Information Processing Systems* (2021).
9. Li Y., Hou Q., Zheng Z., Ming-Ming C., Yang J., Li X. Large Selective Kernel Network for Remote Sensing Object Detection. *arXiv.org*, 2023.
10. Lv R., Wang X., Yang T.: Small Object Detection with Scale Adaptive Balance Mechanism. In: *International Conference on Signal Processing Proceedings*, vol. 1, pp. 361. (2020).
11. Rao X., Zhou L.: Cross-Grid Label Assignment for Arbitrary-Oriented Object Detection in Aerial Images. *IEEE Geoscience and Remote Sensing Letters*. 21. 1 (2024).
12. Yang Y., Ju Y., Zhou Z.: A Super Lightweight and Efficient SAR Image Ship Detector. *IEEE Geoscience and Remote Sensing Letters*. 20. 1 (2023).
13. Wang S., Jiang F., Zhang B., Ma R., Hao Q.: Development of UAV-Based Target Tracking and Recognition Systems. *IEEE Transactions on Intelligent Transportation Systems*. 21. 3409 (2020).
14. Dosovitskiy A., Beyer L., Kolesnikov A., Weissenborn D., Zhai X., Unterthiner T., Dehghani M., Minderer M., Heigold G., Gelly S., Uszkoreit J., Houshy N.: An image is worth 16x16 words: Transformers for image recognition at scale. In: *International Conference on Learning Representations* (2021).
15. Gao L., Liu H., Yang M., Chen L., Wan Y., Xiao Z., Qian Y.: STransFuse: Fusing Swin Transformer and Convolutional Neural Network for Remote Sensing Image Semantic Segmentation. *IEEE Journal of Selected Topics in Applied Earth Observations and Remote Sensing*. 14. 10990 (2021).
16. Liu Z., Lin Y., Cao Y., Hu H., Wei Y., Zhang Z., Lin S., Guo B.: Swin Transformer: Hierarchical Vision Transformer using Shifted Windows. In: *IEEE/CVF International Conference on Computer Vision (ICCV)*, vol. 2021
17. Ding X., Zhang X., Zhou Y., Han J., Ding G., Sun J. Scaling Up Your Kernels to 31x31: Revisiting Large Kernel Design in CNNs. Ithaca: Cornell University Library, *arXiv.org*, 2022.
18. Liu Z., Mao H., Wu C., Feichtenhofer C., Darrell T., Xie S.: A ConvNet for the 2020s. In: *IEEE/CVF conference on computer vision and pattern recognition*, vol. 2022)
19. Liu S., Chen T., Chen X., Chen X., Xiao Q., Wu B., Karkkainen T., Pechenizkiy M., Mocanu D.C., Wang Z.: MORE CONVNETS IN THE 2020S: SCALING UP KERNELS BEYOND 51×51 USING SPARSITY. In: *International Conference on Learning Representations*, vol. 2023)
20. Xu Z., Zhang W., Zhang T., Li J.: HRCNet: High-Resolution Context Extraction Network for Semantic Segmentation of Remote Sensing Images. *Remote Sensing*. 13. 71 (2021).
21. Howard A.G., Zhu M., Chen B., Kalenichenko D., Wang W., Weyand T., Andreetto M., Adam H.: MobileNets: Efficient Convolutional Neural Networks for Mobile Vision Applications. *arxiv*. 2017).
22. Zhang X., Zhou X., Lin M., Sun J.: ShuffleNet: An Extremely Efficient Convolutional Neural Network for Mobile Devices. In: *IEEE/CVF conference on computer vision and pattern recognition*, vol. 2018)

23. Lin J., Zhao Y., Wang S., Tang Y.: YOLO-DA: An Efficient YOLO-Based Detector for Remote Sensing Object Detection. *IEEE Geoscience and Remote Sensing Letters*. 20. 1 (2023).
24. Dong C., Jiang X., Hu Y., Du Y., Pan L.: EL-Net: An efficient and lightweight optimized network for object detection in remote sensing images. *Expert Systems with Applications*. 255. 124661 (2024).
25. Zhu S., Miao M.: SCNet: A Lightweight and Efficient Object Detection Network for Remote Sensing. *IEEE Geoscience and Remote Sensing Letters*. 21. 1 (2024).
26. Yang Y., Sun X., Diao W., Li H., Wu Y., Li X., Fu K.: Adaptive Knowledge Distillation for Lightweight Remote Sensing Object Detectors Optimizing. *IEEE Transactions on Geoscience and Remote Sensing*. 60. 1 (2022).
27. Xie S., Zhou M., Wang C., Huang S.: CSPPartial-YOLO: A Lightweight YOLO-Based Method for Typical Objects Detection in Remote Sensing Images. *IEEE Journal of Selected Topics in Applied Earth Observations and Remote Sensing*. 17. 388 (2024).
28. Ma X., Ji K., Xiong B., Zhang L., Feng S., Kuang G.: Light-YOLOv4: An Edge-Device Oriented Target Detection Method for Remote Sensing Images. *IEEE Journal of Selected Topics in Applied Earth Observations and Remote Sensing*. 14. 10808 (2021).
29. Lin T., Dollar P., Girshick R., He K., Hariharan B., Belongie S.: Feature Pyramid Networks for Object Detection. In: *IEEE/CVF conference on computer vision and pattern recognition*, vol. 936. IEEE, 2017)
30. Liu S., Qi L., Qin H., Shi J., Jia J.: Path Aggregation Network for Instance Segmentation. In: *IEEE/CVF conference on computer vision and pattern recognition*, vol. 2018)
31. Ma Y., Yu M., Lin H., Liu C., Hu M., Song Q.: Efficient analysis of deep neural networks for vision via biologically-inspired receptive field angles: An in-depth survey. *Information Fusion*. 112. 102582 (2024).
32. Gao T., Niu Q., Zhang J., Chen T., Mei S., Jubair A.: Global to Local: A Scale-Aware Network for Remote Sensing Object Detection. *IEEE Transactions on Geoscience and Remote Sensing*. 61. 1 (2023).
33. Han W., Chen J., Wang L., Feng R., Li F., Wu L., Tian T., Yan J.: Methods for Small, Weak Object Detection in Optical High-Resolution Remote Sensing Images: A survey of advances and challenges. *IEEE Geoscience and Remote Sensing Magazine*. 9. 8 (2021).
34. Wang Z., Hua Z., Wen Y., Zhang S., Xu X., Song H.: E-YOLO: Recognition of estrus cow based on improved YOLOv8n model. *Expert Systems with Applications*. 238. 122212 (2024).
35. Xu C., Wang J., Yang W., Yu H., Yu L., Xia G.: Detecting tiny objects in aerial images: A normalized Wasserstein distance and a new benchmark. *ISPRS Journal of Photogrammetry and Remote Sensing*. 190. 79 (2022).
36. Xia G., Bai X., Ding J., Zhu Z., Belongie S., Luo J., Datcu M., Pelillo M., Zhang L.: DOTA: A Large-scale Dataset for Object Detection in Aerial Images. In: *IEEE/CVF conference on computer vision and pattern recognition*, vol. 2018)
37. Cheng G., Zhou P., Han J.: Learning Rotation-Invariant Convolutional Neural Networks for Object Detection in VHR Optical Remote Sensing Images. *IEEE Transactions on Geoscience and Remote Sensing*. 54. 7405 (2016).
38. Ren S., He K., Girshick R., Sun J.: Faster R-CNN: Towards Real-Time Object Detection with Region Proposal Networks. *IEEE Transactions on Pattern Analysis and Machine Intelligence*. 39. 1137 (2017).
39. He K., Gkioxari G., Dollar P., Girshick R.: Mask R-CNN. *IEEE transactions on pattern analysis and machine intelligence*. 42. 386 (2020).

40. Tian S., Kang L., Xing X., Tian J., Fan C., Zhang Y.: A Relation-Augmented Embedded Graph Attention Network for Remote Sensing Object Detection. *IEEE Transactions on Geoscience and Remote Sensing*. 60. 1 (2022).
41. Ge Z., Liu S., Wang F., Li Z., Sun J.: YOLOX: EXceeding YOLO Series in 2021. arxiv. 2021).
42. Lin Q., Zhao J., Du B., Fu G., Yuan Z.: MEDNet: Multiexpert Detection Network With Unsupervised Clustering of Training Samples. *IEEE Transactions on Geoscience and Remote Sensing*. 60. 1 (2022)
43. Liu X., Zhang H., Gong W., Li X.: YOLO-PDNet: Small Target Recognition Improvement for Remote Sensing Image Based on YOLOv8. In: *International Joint Conference on Neural Networks (IJCNN)*, vol. 1. IEEE, 2024)
44. Sun H., Yao G., Zhu S., Zhang L., Xu H., Kong J.: SOD-YOLOv10: Small Object Detection in Remote Sensing Images Based on YOLOv10. *IEEE Geoscience and Remote Sensing Letters*. 22. 1 (2025).
45. Guo D., Zhou Z., Guo F., Jia C., Huang X., Feng J., Shen Z.: A Remote Sensing Target Detection Model Based on Lightweight Feature Enhancement and Feature Refinement Extraction. *IEEE Journal of Selected Topics in Applied Earth Observations and Remote Sensing*. 17. 9569 (2024).
46. Wang P., Sun X., Diao W., Fu K.: FMSSD: Feature-Merged Single-Shot Detection for Multiscale Objects in Large-Scale Remote Sensing Imagery. *IEEE Transactions on Geoscience and Remote Sensing*. 58. 3377 (2020).
47. Azimi S.M., Vig E., Bahmanyar R., Komer M., Reinartz P.: Towards Multi-class Object Detection in Unconstrained Remote Sensing Imagery. In: *Asian Conference on Computer Vision*, vol. 2018)
48. Wang H., Wang H., Wu L.: CMR-net: A cross modality reconstruction network for multi-modality remote sensing classification. *PLOS ONE*. 19. e0304999 (2024).
49. Yan J., Wang H., Yan M., Diao W., Sun X., Li H.: IoU-Adaptive Deformable R-CNN: Make Full Use of IoU for Multi-Class Object Detection in Remote Sensing Imagery. *Remote Sensing*. 11. 286 (2019).
50. Tan M., Pang R., Le Q.V.: EfficientDet: Scalable and Efficient Object Detection. In: *IEEE/CVF conference on computer vision and pattern recognition*, vol. 2020)
51. Wang G., Zhuang Y., Chen H., Liu X., Zhang T., Li L., Dong S., Sang Q.: FSoD-Net: Full-Scale Object Detection From Optical Remote Sensing Imagery. *IEEE Transactions on Geoscience and Remote Sensing*. 60. 1 (2022)